

Molecular beam epitaxy growth of superconducting tantalum germanide

Patrick J. Strohbeen,¹ Aurelia M. Brook,¹ Ido Levy,¹ Wendy L. Sarney,² Jechiel van Dijk,¹ Hayden Orth,¹ Melissa Mikalsen,¹ and Javad Shabani¹

¹*Center for Quantum Information Physics, Department of Physics, New York University, New York, NY 10003 USA*

²*Army Research Directorate, DEVCOM Army Research Laboratory, Adelphi, MD 20783 USA*

(Dated: 5 December 2023)

Developing new material platforms for use in superconductor-semiconductor hybrid structures is desirable due to limitations caused by intrinsic microwave losses present in commonly used III/V material systems. With the recent reports that tantalum provides drastic improvements when implemented in superconducting circuit elements over traditional Nb and Al films, exploring Ta as an alternative superconductor in hybrid material systems seems necessary. Here, we present our study on the growth of Ta on semiconducting Ge (001) substrates grown via molecular beam epitaxy. We show that the Ta diffuses into the Ge matrix in a self-limiting nature resulting in extremely smooth and abrupt surfaces and interfaces that are ideal for future cQED device fabrication. The films have a nominal composition of TaGe₂ and form a native oxide of nominal composition Ta₂Ge₂O₅ that also forms a sharp interface with the underlying film. These films are superconducting with a $T_C \sim 1.8 - 2\text{K}$ and $H_C^\perp \sim 1.88\text{T}$, $H_C^\parallel \sim 5.1\text{T}$.

Superconductor-semiconductor (S-Sm) hybrid material platforms have been of interest in the last few decades for studying mesoscopic superconductor physics¹, the search for topological superconductivity^{2,3}, and most recently for the development of new voltage-tunable qubits, couplers, and other superconducting circuit elements⁴⁻⁶. However, due to the complexity of the material requirements (e.g. interface roughness, band alignment, etc.), growth of these structures is not straightforward. Furthermore, in terms of the latter application in superconducting circuitry for circuit quantum electrodynamics (cQED) applications, high intrinsic losses in the community standard Al-InAs system⁴ have motivated material exploration studies to search for materials better suited towards these cQED applications. On the other hand, recent advancements in the Si-Ge alloy system present these materials to be highly promising for low-microwave loss materials^{7,8} for quantum information applications.

In terms of superconducting materials, implementation of tantalum metal is also extremely interesting for cQED devices due to the fact that it forms a well-behaved native oxide for superconducting microwave applications⁹⁻¹¹. Additionally, recent studies showed that this behavior of Ta also propagates to high-performance cQED devices^{12,13}. In this context, major increases in qubit coherence times are caused by low intrinsic two-level system (TLS) losses within the Ta metal native oxide, Ta₂O₅. However, implementation of this material into S-Sm hybrid materials requires significant effort in terms of understanding the film growth parameters to promote smooth interfaces/surfaces. Thus, further study of Ta and Ta-alloys is of interest for investigation of new superconductor-semiconductor (S-Sm) hybrid material systems.

Here, we report the first diffusion-limited growth (diffusion-growth) of tantalum germanide films via molecular beam epitaxy (MBE). We evaluate our grown films via a suite of structural and electronic materials characterization and present the chemical composition, structure, and superconductivity behavior of this material. We present a unique growth method that forms uniform, wafer-scale thin films of homogeneous chemical composition and thickness that make

this material system highly promising for future application in superconducting cQED devices.

The tantalum germanide films are grown on 50.8mm Ge(001) substrates in a custom solid-source molecular beam epitaxy system (Mod Gen II) equipped with three electron beam sources and hydrogen cleaning capabilities. The internal manifold around the sources is water-cooled and no LN₂ cryo-paneling is used during this deposition. The substrates are first etched *ex-situ* in deionized water at 90°C for 15 minutes and then immediately loaded into vacuum on indium-free blocks. The substrates are initially outgassed in the growth reactor at 200°C for 15 minutes, before slowly increasing temperature to 550°C to anneal for 10 minutes. Ta deposition was done using a water-cooled vertical EB-V e-beam source from MBE Komponenten at an emission current of 180mA in a 6kV acceleration field. The films are grown at 400°C, immediately following the Ge oxide removal. Due to passive heating from the Ta source, deposition was conducted in three cycles of 10 minutes each, allowing the chamber to cool for 15 minutes between deposition cycles to prevent significant outgassing from the chamber walls.

Figure 1 presents x-ray diffraction data taken using a Bruker D8 Discovery lab source diffractometer with a da Vinci configuration and a conditioned Cu K α_1 source. A collimator and 1mm slit are used to reduce the effects of substrate bowing in select measurements. All scans are measured in a double crystal configuration. An out-of-plane $\theta - 2\theta$ scan is presented in Fig. 1a in which the only reflection visible is the substrate Ge (004) reflection at 66deg. X-ray reflectivity (XRR) measurements are taken after removing the collimator and reducing the slits to 0.2mm. The XRR results are presented in Figure 1b, showing extremely sharp interfaces for the amorphous film. The fit is initialized assuming a two-layer model for the film structure with the primary layer being a film of tantalum germanide and the secondary layer being a thin native oxide layer. Since the density is unknown due to the amorphous nature, we allow the scattering length density (SLD) to vary in the fitting procedure as well. The results of the fit are shown below in table I. The feature that is

not captured by our fitting model we speculate is related to the dot-like features observed in the atomic force microscopy (AFM) image seen in Figure 1c. These features are well dispersed across the sample surface and are all nominally a uniform thickness and may be the cause of this spurious peak that is not captured by our two-layer model. The roughness values for the fits are initialized at 7 Å, the roughness we measured in AFM, but then is allowed to vary for both layers individually.

Layer	SLD ($10^{-6}/\text{\AA}^2$)	thickness (Å)	Roughness (Å)
Tantalum Germanide	93.97	175.1	3.6
Native Oxide	64.95	24.4	9.3

TABLE I. X-ray reflectivity fitting results.

From the fits we extract scattering length densities (SLD) for total internal reflection x-ray scattering in the XRR measurements. Using Eqn. 1 below we then calculate the product of $\rho f_1/M_a$, relating the SLD from the fit back to the material density and scattering factor.

$$Re(SLD) = \frac{\rho N_a r_e}{M_a} f_1 \quad (1)$$

Where ρ is the material density, N_a is Avogadro's constant, r_e is the classical electron radius $\sim 2.818 \times 10^{-15}$ m, M_a is the molar mass, and f_1 is the real part of the atomic scattering factor of the compound. We calculate values of 5.54 cm^{-3} and 3.83 cm^{-3} for the tantalum germanide and native oxide layers, respectively.

Crystallinity and composition of the tantalum germanide film is examined with scanning transmission electron microscopy (STEM) in a JEOL ARM200F, equipped with a spherical aberration corrector for probe mode, and operated at 200 keV. The samples were prepared with cross-sectional tripod polishing to 20 μm thickness, followed by shallow angle Ar⁺ ion milling with low beam energies([1]3 keV), and LN2 stage cooling in a PIPS II ion mill. Exemplary transmission electron microscopy images are shown in Figure 2, where we observe sharp interfaces and well-defined film and oxide regions of thicknesses $\sim 18.7 \text{ nm}$ and 2.2 nm , respectively, in good agreement with our XRR fitting. To calculate the material density, rough estimations of film composition are obtained from energy dispersive x-ray spectroscopy (EDS) as shown in Figure 2b. From EDS we estimate the tantalum germanide phase to be $\sim 36 : 74$ Ta:Ge ratio and the native oxide to have a composition of $\sim 56 : 22 : 22$ O:Ta:Ge. From these compositions we see that the film and native oxide layers have approximate chemical formulations of TaGe_2 and $\text{Ta}_2\text{Ge}_2\text{O}_9$, respectively. Interestingly, this implies that the oxide is made up of a mixture of one part Ta_2O_5 and two parts GeO_2 .

Assuming random distribution of elemental species in the two distinct layers, we then calculate average material densities to be 13.97 g/cm^3 and 9.47 g/cm^3 for the TaGe_2 and oxide layers, respectively. We attribute the larger density than reported literature values for TaGe_2 (11.43 g/cm^{315}) to a Ta-rich

phase, likely due to small regions of non-reacted Ta metal. Interestingly, the calculated density of the oxide layer is significantly larger than reports of Ta_2O_5 and GeO_2 , which are 8.31 g/cm^{316} and 6.27 g/cm^{317} , respectively. However, there are reports of high pressure phases of the tantalum pentoxide in which the densities are drastically increased¹⁸ up to 10.75 g/cm^3 . Therefore, we speculate the nature of this oxide layer to be the result of residual internal strains inducing the formation of small regions of high density polymorphs of the Ta_2O_5 and GeO_2 native oxide phases.

Magnetotransport measurements of this material are done in an Oxford Triton dry dilution refrigerator with a base temperature of 15mK and a single direction magnet with a maximum field of 14T. Samples are cleaved down to roughly 5x5mm chips. Contacts on the chip are made by annealing In-Sn eutectic into the four corners in a Van der Pauw geometry which are then contacted to the sample board via gold wires. The results of these measurements are presented in Figure 3. We see a sharp transition to a zero resistance state at roughly 2K upon cooldown, as shown in Figure 3a. To investigate the field dependence, we sweep out-of-plane and in-plane magnetic field as shown in Figs. 3b and c, respectively. The resistance surface presented in Fig. 3b shows a very sharp transition from the superconducting phase to the normal state, suggestive of type 1 superconductivity. This is observed in the tight spread of $0.9R_n$, $0.5R_n$, and $0.1R_n$ contours overlaid on the color map. For out-of-plane field configuration we observe a critical applied field of $H_C \sim 1.88T$. The critical field fitting gives us a critical temperature of roughly 1.8K. With an in-plane field configuration we measure a critical applied field of $H_C \sim 5.1T$ that also exhibits a sharp superconducting transition up to 1K. We present this data in Fig. 3c in which we overlay the $0.9R_n$, $0.5R_n$, and $0.1R_n$ contours. The variation in sheet resistance between Fig. 3b and Figs. 3a and c are a result of oxidation in the film over the course of roughly six months causing a slight increase in film resistance. The measurements were otherwise conducted on the exact same sample.

In conclusion, we presented here the growth, structure, and transport characteristics of diffusion-grown tantalum germanide thin films grown via MBE. The tantalum germanide films are formed by a rate-limited diffusion process in which the e-beam evaporated Ta diffuses into the surface such that a nominal composition of 1 : 2 of Ta : Ge is maintained within the film region. These films form a small native oxide layer with sharp interfaces that has a composition that suggests the formation of both Ta_2O_5 and GeO_2 , also in a ratio of 1 : 2. Transport shows a reasonable critical temperature of ~ 1.8 -2K, but more we find a critical out-of-plane and in-plane critical field of $H_C^\perp \sim 1.88T$ and $H_C^\parallel \sim 5.1T$, respectively. With such a high critical field and the ease of semiconductor integration, this new superconducting material is interesting to study cQED devices.

ACKNOWLEDGMENTS

The authors would like to acknowledge funding support for this project by AFOSR award FA9550-21-1-0338.

- ¹F. Rahman, T. J. Thornton, R. Huber, L. F. Cohen, W. T. Yuen, and R. A. Stradling, “Superconductor-semiconductor interaction effects in mesoscopic hybrid structures,” *Phys. Rev. B* **54**, 14026–14031 (1996).
- ²V. Mourik, K. Zuo, S. M. Frolov, S. R. Plissard, E. P. A. M. Bakkers, and L. P. Kouwenhoven, “Signatures of majorana fermions in hybrid superconductor-semiconductor nanowire devices,” *Science* **336**, 1003–1007 (2012).
- ³E. Prada, P. San-Jose, M. W. A. de Moor, A. Geresdi, E. J. H. Lee, J. Klinovaja, D. Loss, J. Nygård, R. Aguado, and L. P. Kouwenhoven, “From andreev to majorana bound state in hybrid superconductor-semiconductor nanowires,” *Nat. Rev. Phys.* **2**, 575–594 (2020).
- ⁴L. Casparis, M. R. Connolly, M. Kjaergaard, N. J. Pearson, A. Kringhøj, T. W. Larsen, F. Kuemmeth, T. Wang, C. Thomas, S. Gronin, G. C. Gardner, M. J. Manfra, C. M. Marcus, and K. D. Petersson, “Superconducting gatemon qubit based on a proximitized two-dimensional electron gas,” *Nat. Nanotechnol.* **13**, 915–919 (2018).
- ⁵G. Burkard, M. J. Gullans, X. Mi, and J. R. Petta, “Superconductor-semiconductor hybrid-circuit quantum electrodynamics,” *Nat. Rev. Phys.* **2**, 129–140 (2020).
- ⁶W. M. Strickland, B. H. Elfeky, J. O. Yuan, W. F. Schiela, P. Yu, D. Langone, M. G. Vavilov, V. E. Manucharyan, and J. Shabani, “Superconducting resonators with voltage-controlled frequency and nonlinearity,” *Phys. Rev. Appl.* **19**, 034021 (2022).
- ⁷M. Sandberg, V. P. Adiga, M. Brink, C. Kurter, C. Murray, M. Hopstaken, J. Bruley, J. S. Orcutt, and H. Paik, “Investigating microwave loss of sig using superconducting transmon qubits,” *Appl. Phys. Lett.* **118**, 124001 (2021).
- ⁸G. Scappucci, C. Kloeffer, F. A. Zwanenburg, D. Loss, M. Myronov, J.-J. Zhang, S. D. De Franceschi, G. Katsaros, and M. Veldhorst, “The germanium quantum information route,” *Nat. Rev. Mater.* **6**, 926–943 (2021).
- ⁹L. Y. L. Shen, *Superconductivity in d- and f-Band Metals*, edited by D. H. Douglass (Springer, 1972).
- ¹⁰E. G. Spencer and J. M. Rowell, “Superconductivity of ta-zr films produced by co-sputtering,” *IEEE Trans. Magn.* **MAG-17**, 322–325 (1981).
- ¹¹D. W. Face, D. E. Prober, W. R. McGrath, and P. Richard, “High quality tantalum superconducting tunnel junctions for microwave mixing in the quantum limit,” *Appl. Phys. Lett.* **48**, 1098–1100 (1986).
- ¹²A. P. M. Place, L. V. H. Rodgers, P. Mundada, B. M. Smitham, M. Fitzpatrick, Z. Leng, A. Premkumar, J. Bryon, A. Vrajitoarea, S. Sussman, G. Cheng, T. Madhavan, H. K. Babla, X. H. Le, Y. Gang, B. Jäck, A. Gye-nis, N. Yao, R. J. Cava, N. P. de Leon, and A. A. Houck, “New material platform for superconducting transmon qubits wit coherence times exceed-ing 0.3 milliseconds,” *Nat. Commun.* **12**, 1779 (2021).
- ¹³R. A. McLellan, A. Dutta, C. Zhou, Y. Jia, C. Weiland, X. Gui, A. P. M. Place, K. D. Crowley, X. H. Le, T. Madhavan, Y. Gang, L. Baker, A. R. Head, I. Waluyo, R. Li, K. Kisslinger, A. Hunt, I. Jarrige, S. A. Lyon, A. M. Barbour, R. J. Cava, A. A. Houck, S. L. Hulbert, M. Liu, A. L. Walter, and N. P. de Leon, “Chemical profiles of the oxides on tantalum in state of the art superconducting circuits,” *Advanced Science* **10**, 2300921 (2023).
- ¹⁴G. Vignaud and A. Gibaud, “REFLEX: a program for the analysis of specular X-ray and neutron reflectivity data,” *J. Appl. Cryst.* **52**, 201–213 (2019).
- ¹⁵L. H. Brixner, “X-ray study and thermoelectric properties of the NbSi_xGe_{2-x} and the TaSi_xGe_{2-x} systems,” *J. Inorg. Nucl. Chem.* **25**, 257–260 (1963).
- ¹⁶N. C. Stephenson and R. S. Roth, “Structural Systematics in the Binary System Ta₂O₅-WO₃. V. The Structure of the Low-Temperature Form of Tantalum Oxide *L*-Ta₂O₅,” *Acta Cryst.* **B27**, 1037–1044 (1971).
- ¹⁷W. H. Baur and A. A. Khan, “Rutile-Type Compounds. IV. SiO₂, GeO₂ and a Comparison with other Rutile-Type Structures,” *Acta Cryst.* **B27**, 2133–2139 (1971).
- ¹⁸I. P. Zibrov, V. P. Filonenko, M. Sundberg, and P.-E. Werner, “Structures and phase trasiitions of B-Ta₂O₅ and Z-Ta₂O₅: two high-pressure forms of Ta₂O₅,” *Acta Cryst.* **B56**, 659–665 (2000).

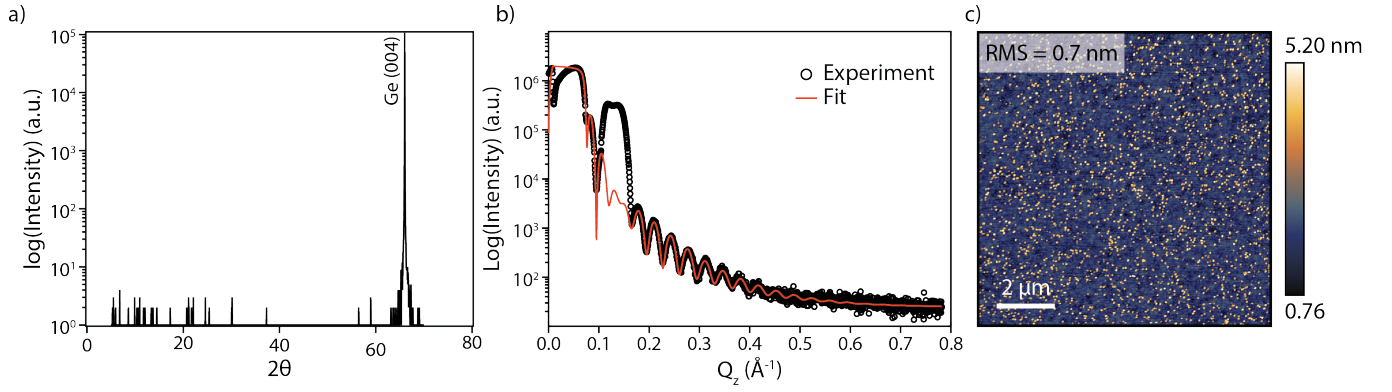


FIG. 1. X-ray diffraction characterization of tantalum germanide film. **(a)** Out-of-plane θ - 2θ scan. The only distinct reflection is from the Ge substrate. **(b)** X-ray reflectivity measurement of the tantalum germanide film. The fit is done using REFLEX¹⁴ standalone reflectivity fitting software, assuming two layers of composition TaGe_2 and $\text{Ta}_2\text{Ge}_2\text{O}_9$. **(c)** $10\mu\text{m} \times 10\mu\text{m}$ AFM image of tantalum germanide surface. RMS value of 7 \AA was used as the initial roughness for the XRR fitting.

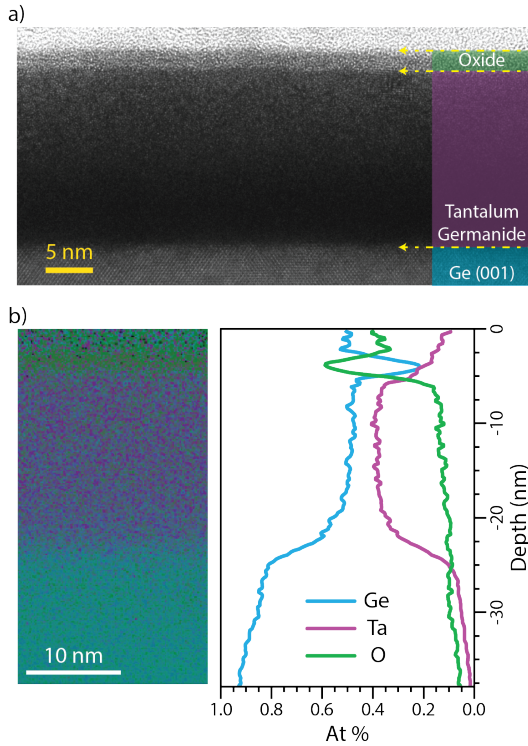


FIG. 2. TEM imaging of tantalum germanide film. **(a)** Zoomed-out image of tantalum germanide lamella that shows sharp interfaces at the oxide-film and film-substrate interfaces. **(b)** EDS measurement of the film and native oxide regions. The line traces on the right are an average across the entire window presented in the left side.

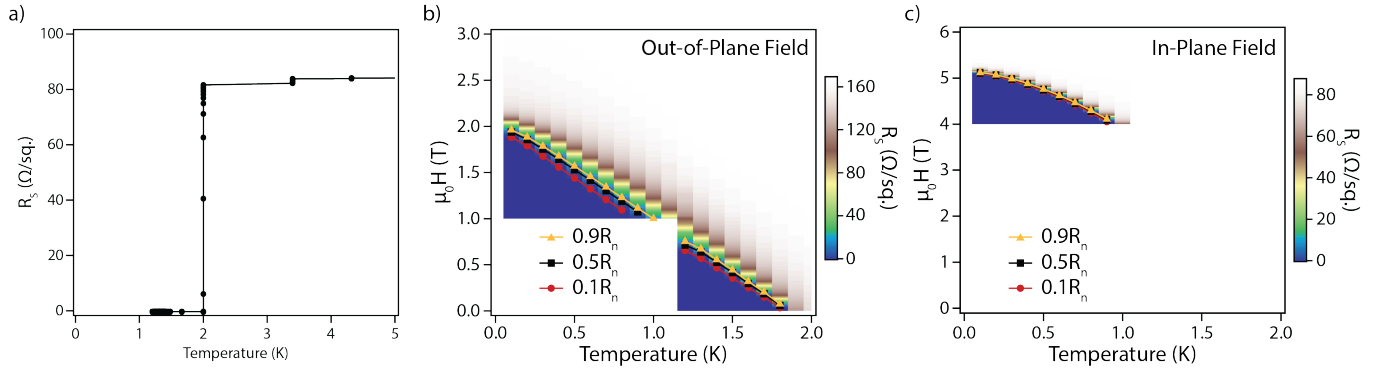


FIG. 3. Magnetotransport data of tantalum germanide film. **(a)** Cooldown trace of sheet resistance, R_S . We see a zero-resistance transition near 2K. **(b)** R_S map as a function of applied out-of-plane field and temperature. Lines are fits to the $0.9R_n$, $0.5R_n$, and $0.1R_n$ values. **(c)** R_S map for in-plane magnetic field configuration.